doi:10.6041/j.issn.1000-1298.2016.03.036

Estimation Models of Above-ground Dry Matter Accumulation of Summer Maize Based on Hyperspectral Remote Sensing Vegetation Indexes

Liu Bingfeng[1] Li Jun[1] He Jia[2] Shi Zujiao[1]

(1. *College of Agronomy*, *Northwest A&F University*, *Yangling*, *Shaanxi* 712100, *China*
2. *Agricultural Economy and Information Research Institution*, *Henan Academy of Agricultural Sciences*, *Zhengzhou* 450002, *China*)

Abstract: An on-site field experiment, which includes five nitrogen fertilizer application rate treatments, four phosphorus fertilizer application rate treatments and two summer maize cultivars treatments, was conducted at agricultural experimental station of Northwest A&F University during 2011—2014. Summer maize canopy spectral reflectance and above-ground dry matter accumulation (ADMA) were measured at the huge bellbottom stage, silking stage, filling stage and maturity stage of summer maize. 21 canopy vegetation indexes of hyperspectral remote sensing in 2011 and 2013 were chosen to establish liner, logarithmic, quadratic and exponential regression relationship between ADMA and canopy spectral parameters for each cultivar. Different regression models were applied to establish the relationship between spectrum vegetation indexes and summer maize ADMA. Three models with high coefficients and *F* values at each growth stage were chosen to verify root mean square error and relative error with data of canopy spectral reflectance and ADMA in 2012 and 2014 separately. The smallest root mean square error and relative error models were chosen as the best models for estimation ADMA of maize. The results show that, at the huge bellbottom stage, filling stage and maturity stage of maize, spectrum vegetation indexes for the best fitting regression relationship models with ADMA were GNDVI, PSSRc, NDVI4 and DI. These models could be used as the best models for the estimation of summer maize above-ground ADMA.

Key words: summer maize; canopy; above-ground dry matter accumulation; hyperspectral remote sensing vegetation indexes; estimation model

0 Introduction

Crop canopy spectral analysis is recognized as a non-destructive testing technology of remote sensing which offers an opportunity for indicating information of vegetation properties, photosynthetic biomass accumulation and other indexes after using hyperspectral technology to monitor physical and chemical parameters of crop by constituting the vegetation index of linear and nonlinear combination of hyperspectral data[1].

Above-ground dry matter accumulation (ADMA) is the basis for the formation of crop yield during crop growth period. Estimation of crop dry matter accumulation by hyperspectral remote sensing vegetation index makes remote sensing for dynamic monitoring of crop growth and yield inversion come true. Depending on normalized difference vegetation index (NDVI), ZHANG et al.[2] established a model for above-ground biomass in Poyang Lake region. WANG[3] using the components of biomass (leaves and the quality of stem and pod) of rape established regression model with RVI and NDVI respectively. SHIBAYAMA et al.[4] adopted the ratio index (R_{1100}/R_{1200}) simulation to simulate and predict the dry mass of double cropping of rice well. The studies of SONG et al.[5] have shown that RVI (R_{760}/R_{710}) can simulate soybean's fresh matte accumulation of the over ground part. Based on the studies of winter wheat biomass model (WBM), ZHUANG et al.[6] believes that using NDVI transformation model of satellite images can better simulate biomass of winter wheat, and can accurately obtain different levels of biomass growing information in a large area. The studies of

Received date: 2015-09-08 Accepted date: 2015-12-18
Supported by National Hi-tech Research and Development Program of China (863 Program) (Grant No. 2013AA102902), and National Natural Science Foundation of China (Grant Nos. 31571620, 31071374)
Corresponding author: Li Jun, Professor. E-mail: junli@nwsuaf.edu.cn. Tel: +86-13002963615

CHU et al.[7-8] indicated that estimating the aboveground biomass of the Qinghai-Tibet region through varieties of vegetation index models are possible. These studies were based on the spectral simulation to estimate biomass at lower biomass conditions, but the applicability of the model is reducing at a higher biomass conditions due to spectrum model saturation[9-12].

In summary, an increasing number of scholars deem that above-ground biomass of different kinds of vegetation can be predicted through varieties of vegetation index models and have made considerable achievements, while researches on spectrum model to estimate high biomass are relatively small, especially in summer corn. This article predictes and simulates above-ground biomass of summer corn, then simultaneously set and verifies summer corn above-ground dry biomass regression model based on vegetation index through different band combinations of hyperspectral vegetation index and normalized difference vegetation index. The specific objectives of this study are to provide evidence for hyperspectral remote sensing of summer corn growing and provide a realistic foundation for using spectral vegetation index to estimate higher biomass.

1 Material and methods

1.1 Site description and experimental design

A field experiment of summer maize growing hyperspectral remote sensing was conducted from 2011 to 2014 at a site in Northwest A&F University North Campus (34°29′N, 108°06′E; elevation 400 m) where is the warm temperate semi-humid climate in this area. The soil at the study site is Hongyou soil which has a silt loam texture. Soil organic carbon content, total nitrogen, available nitrogen and available phosphorus at 0 ~ 20 cm depth were 10.48 g/kg, 1.20 g/kg, 36.48 mg/kg, and 12.49 mg/kg respectively.

Different nutrient levels of nitrogen, phosphorus and varieties of summer maize were set at the study site. We took Split-split Plot Design and applied multi-year fertilizer treatments researches in the field, arranging nitrogen as main treatment, phosphate as secondary treatment and variety as tertiary. In this experiment, five treatments (N0, N1, N2, N3, N4) of nitrogen fertilizer were designed which applied 0, 75, 150, 225, 300 kg/hm^2 nitrogen respectively, and 60% of the total nitrogen fertilizer as basal, 40% as top dressing. Set 4 treatments (P0, P1, P2, P3) of phosphate which applied 0, 60, 120, 180 kg/hm^2 P_2O_5 respectively, and phosphate fertilizer was applied at once as base fertilizer. Two tested summer maize were Yuyu 22 (horizontal leaf type) and Zhengdan 958 (compact type), which at a density of 52 500 plants/hm^2 and 67 500 plants/hm^2 respectively.

1.2 Parameter and determination methord

1.2.1 Measurement of corn reflectance

Summer maize canopy spectral reflectance were measured with ASD fieldSpec3 hyperspectral instrument at the huge bellbottom stage (July 15), silking stage (August 2), filling stage (August 17) and maturity stage (September 10) of maize at 10:30—13:30 on the cloudless, windless weather. Three times of repeat were sampled randomly from each plot, every repeat as one group for 10 times, and the average of the repeat as a canopy spectral reflectance.

1.2.2 Above-ground dry matter and total nitrogen measurement

After field spectrum measurement, cut the above-ground fresh biomass at the measurement area immediately and took them back to thelaboratory, then weighed them after de-enzyme and drying. At last, measured the total nitrogen with Kjeldahl instrument.

1.3 Establishment and precision inspection of hyperspectral remote sensing estimation model

Fitting model including: simple linear function $y = c + ax$; logarithmic function $y = c + a\ln x$; parabola $y = c + ax + bx^2$; exponential function $y = ce^{ax}$. Where y is the above-ground dry weight fitting value, x is spectral variable, c is a constant, and a, b is equation parameters.

Root mean square error (RMSE) evaluation and mean relative error evaluation (RE): the parameters estimated from the univariate and multivariate regression model which can evaluate by the root-mean-square deviation of precision.

$$V_{\mathrm{RMSE}} = \sqrt{\sum_{i=1}^{n} (y_i - \hat{y}_i)^2 / n}$$

$$V_{RE} = (y_i - \hat{y}_i)/y_i \times 100\%$$

Where y_i is measured value, y is predicted value, n is

sample number.

1.4 Selection of vegetation index

Based on the existing research results, 21 ratio vegetation index and normalized difference vegetation index of summer maize were selected to establish the above-ground dry matter hyperspectral remote sensing monitoring model (Tab. 1). In addition, 21 ratio vegetation indexes and normalized difference vegetation index were greenness index(GI), pigment simple ratio index a, b and c(PSSRa, PSSRb, PSSRc), simple pigment ratio index(SRPI), difference index(DI), difference vegetation index(DVI), double difference index (DD), moderate resolution imaging land chlorophyll index (MTCI), NDVI, chlorophyll normalized difference vegetation index (NPCI), normalized magnesium removal effect index(NPQI), photochemical reflectance index (PRI), structural reinforcement pigment index(SIPI), improved red edge ratio vegetation index (MSR750), plant senescence index (PSRI), red-green ratio index (RGR), and normalized difference vegetation index 1, 2, 3 and 4 (NDVI1, NDVI2, NDVI3, NDVI4).

Tab. 1 Published hyperspectral vegetation indices evaluated in this study

Vegetation Index	The Formula	Literature No.
GI	$R = R_{554}/R_{677}$	[13]
PSSRa	$R = R_{800}/R_{680}$	[14]
PSSRb	$R = R_{800}/R_{635}$	[14]
PSSRc	$R = R_{800}/R_{470}$	[14]
SRPI	$R = R_{430}/R_{680}$	[15]
DI	$R = R_{800} - R_{550}$	[16]
DVI	$R = R_{800} - R_{680}$	[17]
DD	$R = (R_{750} - R_{720}) - (R_{700} - R_{670})$	[18]
MTCI	$R = (R_{750} - R_{710})/(R_{710} - R_{680})$	[19]
NDVI	$R = (R_{801} - R_{550})/(R_{800} + R_{550})$	[20]
NPCI	$R = (R_{680} - R_{430})/(R_{680} + R_{430})$	[23]
NPQI	$R = (R_{415} - R_{435})/(R_{415} + R_{435})$	[21]
PRI	$R = (R_{531} - R_{570})/(R_{530} + R_{570})$	[22]
SIPI	$R = (R_{800} - R_{445})/(R_{800} - R_{680})$	[23]
MSR705	$R = (R_{750} - R_{445})/(R_{705} - R_{445})$	[24]
PSRI	$R = (R_{680} - R_{500})/R_{750}$	[24]
RGR	$R = (R_{612} + R_{660})/(R_{510} + R_{560})$	[25]
NDVI 1	$R = (R_{760} - R_{708})/(R_{760} + R_{708})$	[25]
NDVI 2	$R = (R_{800} - R_{600})/(R_{800} + R_{600})$	[26]
NDVI 3	$R = (R_{900} - R_{680})/(R_{900} + R_{680})$	[27]
NDVI 4	$R = (R_{780} - R_{550})/(R_{780} + R_{550})$	[28]

Note: R_{554} represents spectral reflectance in 554 nm band, rest on.

2 Results and analysis

2.1 Effect of different nitrogen and phosphorus levels on above-ground dry biomass at each growth stage

Took the average of filed experimental data of summer maize from the year 2011 to 2013 as example, analyzed dynamic changing about above-ground dry biomass and total nitrogen under different fertilization treatments (Tab. 2). Above-ground dry biomass during the summer maize growing seasons trend to increasing and reaching the maximum value at filling stage, while the total nitrogen decreased gradually. Silking stage to filling stage of maize were the peak of nutrient absorption and accumulation. At the beginning of silking stage, inner nutrients of corn transfer to ear, reducing the assimilation rate[29], that is the reason why above-ground dry biomass growth rate was declined at latter of filling stage, and different fertilization treatments with similar trends [30].

At the same phosphate level, all of above-ground dry biomass is significantly increased ($P < 0.05$) with the increasing of nitrogen. The study of Al ABBAS et al. also proved that more nitrogen can significantly increase the above-ground dry biomass[31]. At the same level of nitrogen, with the increasing of phosphorus, above-ground dry biomass is also increased. The above-ground dry biomass of high nitrogen and phosphorus treatment (P2N3, P2N4, P3N3, P3N4) were higher than low nitrogen and phosphorus treatment (P0N0, P0N1, P1N0, P1N1). Such as high nitrogen and phosphorus treatment and low nitrogen and phosphorus treatment at silking stage, the above-ground dry biomass was differ 6.88, 5.35, 6.43, 5.80 t/hm^2 respectively, the total nitrogen was differ from 0.83%, 0.58%, 0.77%, 0.69% respectively.

At each growth stage, there were high correlation coefficient between above-ground dry biomass and nitrogen content, both of them were appeared similar trends which increased with fertilizer and had significant difference under the affecting of the treatment of nitrogen and phosphorus coupling process.

2.2 Summer maize canopy spectral reflectance under different fertilization levels of nitrogen and phosphorus

Took summer maize canopy spectral reflectance at

Tab. 2 ADMA and total nitrogen content of canopy under different fertilization treatment at different growth stages of maize

Fertilization treatment		Huge bellbottom stage		Silking stage		Filling stage		Maturity stage	
		Dry biomass/ ($t \cdot hm^{-2}$)	Total nitrogen/%	Dry biomass/ ($t \cdot hm^{-2}$)	Total nitrogen/%	Dry biomass/ ($t \cdot hm^{-2}$)	Total nitrogen/%	Dry biomass/ ($t \cdot hm^{-2}$)	Total nitrogen/%
P0	N0	11.64^{d}	1.13^{c}	18.38^{d}	1.04^{b}	32.54^{d}	0.96^{c}	37.90^{c}	0.84^{d}
	N1	13.09^{c}	1.34^{b}	21.09^{c}	1.39^{a}	35.14^{c}	1.08^{b}	41.68^{b}	0.90^{cd}
	N2	13.79^{b}	1.36^{b}	21.32^{b}	1.41^{a}	35.81^{c}	1.07^{b}	42.13^{b}	1.00^{bc}
	N3	13.78^{b}	1.41^{b}	21.65^{a}	1.48^{a}	40.48^{b}	1.25^{a}	42.35^{b}	1.12^{ab}
	N4	16.35^{a}	1.69^{a}	22.12^{a}	1.53^{a}	42.93^{a}	1.31^{a}	44.42^{a}	1.24^{a}
P1	N0	12.14^{d}	1.27^{d}	19.01^{e}	1.26^{c}	36.20^{d}	1.17^{c}	39.65^{c}	1.18^{c}
	N1	14.10^{c}	1.50^{bc}	20.92^{d}	1.44^{b}	36.15^{d}	1.19^{c}	43.18^{be}	1.27^{b}
	N2	14.07^{c}	1.46^{c}	21.20^{c}	1.43^{b}	40.64^{c}	1.36^{b}	44.04^{b}	1.26^{b}
	N3	14.96^{b}	1.58^{b}	21.92^{b}	1.58^{a}	41.79^{b}	1.39^{ab}	46.63^{a}	1.39^{a}
	N4	17.04^{a}	1.81^{a}	22.50^{a}	1.63^{a}	45.74^{a}	1.51^{a}	46.87^{a}	1.41^{a}
P2	N0	12.55^{d}	1.47^{d}	19.74^{d}	1.49^{c}	37.84^{d}	1.31^{c}	40.86^{d}	1.24^{b}
	N1	14.46^{c}	1.64^{c}	20.04^{d}	1.50^{c}	40.18^{c}	1.45^{b}	43.11^{c}	1.34^{ab}
	N2	15.19^{c}	1.80^{b}	24.19^{c}	1.83^{b}	48.08^{b}	1.72^{a}	48.86^{b}	1.44^{a}
	N3	17.11^{b}	1.96^{a}	25.26^{b}	1.87^{b}	47.73^{b}	1.70^{a}	48.61^{b}	1.47^{a}
	N4	17.93^{a}	2.07^{a}	26.44^{a}	1.97^{a}	50.66^{a}	1.76^{a}	51.60^{a}	1.52^{a}
P3	N0	12.70^{e}	1.69^{e}	20.96^{d}	1.69^{b}	40.55^{d}	1.35^{d}	40.99^{e}	1.27^{c}
	N1	14.37^{d}	1.85^{d}	21.41^{c}	1.69^{b}	41.69^{c}	1.62^{c}	44.36^{d}	1.47^{b}
	N2	15.63^{c}	2.01^{c}	25.00^{b}	1.99^{a}	45.32^{b}	1.68^{bc}	47.31^{c}	1.56^{ab}
	N3	17.27^{b}	2.16^{b}	25.44^{b}	2.03^{a}	45.38^{b}	1.77^{b}	49.57^{b}	1.71^{a}
	N4	18.77^{a}	2.37^{a}	26.72^{a}	2.13^{a}	51.11^{a}	1.97^{a}	54.02^{a}	1.79^{a}
Coefficient correlation r		0.887		0.930		0.940		0.862	

Note: After the column data with different letters indicate differences among treatments at 5% significance level.

silking stage of Zhengdan 958 in a year 2013 as example, analyzed summer maize canopy spectral reflectance changing trend under different levels of nitrogen and phosphorus (Fig. 1). Summer maize canopy spectral reflectance in the 350 nm to 2 350 nm band was trend to similar basically. Summer maize canopy spectral reflectance is lower in 350 nm to 680 nm band, spectral reflectance lower, about 550 nm is chlorophyll strong reflection peak (green peak) which the spectral reflectance about 8% to 12%. Absorption valley, the result of absorbing red light of chlorophyll in photosystem, located in about 680 nm band. At 680 nm to 750 nm band, spectral reflectance climb straight, that is the characteristic spectrum red edge of green plants, strongly absorbing of chlorophyll in red band and more than once scatter of near-infrared light inside the leaves formed the band feature which is an important indicator to describe the health of the crop. There is a stable platform for reflection in the near infrared (750 nm to 1 150 nm), canopy spectralreflectance trend stable (36% to 42%). In 1 150 nm to 2 350 nm band, spectral reflectance is decreased gradually, and about 2 200 nm and 1 700 nm have two reflection peaks, at around 1 400 nm and 1 900 nm is water sub-total absorption bands due to the greater influence of water vapour, which has been struck.

Under different nitrogen and phosphorus levels,

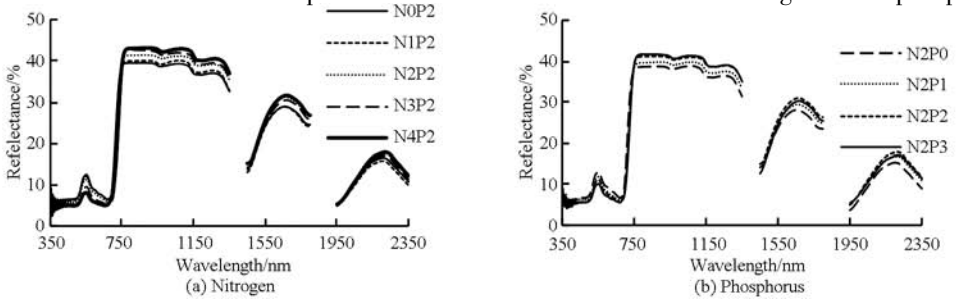

Fig. 1 Change of canopy spectral reflectance of summer maize under different N, P application rates

summer corn canopy spectral reflectance response curve were trend similar. In visible wavelengths (350 ~ 680 nm), spectral reflectance is decreasing with the increasing of nitrogen and phosphorus applied, however, it is opposite in the near infrared (750 ~ 1 350 nm). There is no obvious rules after the 1 350 nm band between spectral reflectance and nitrogen and phosphorus fertility gradient.

2.3 Reflectance between correlation canopy spectral and aboveground dry biomass

According to the reflectance analysis of the independent experimental spectral reflectance data and above-ground dry biomass (Fig. 2), analyze the dynamics correlation between canopy reflectance and above-ground dry biomass of summer corn. As is shown in Fig. 2, at the range 350 nm to 2 350 nm bands, spectral, aboveground dry weight and total nitrogen correlation curve looked similar, and the correlation coefficient average difference was little, further suggested that there were high similarity between the above-ground dry biomass and total nitrogen and the correlation of spectral reflectance.

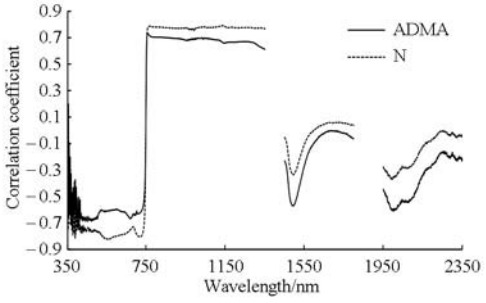

Fig. 2 Correlation coefficient between original spectral reflectance and ADMA, N content of summer maize canopy at different growth stages of maize

At 430 nm to 720 nm band, there were high negative correlation between original canopy spectral reflectance and the above-ground dry biomass of summer corn, that formed a stable platform with correlation coefficient were −0.593 to −0.687. In the position of red edge, obviously, all correlation coefficient appeared undulation, and the relevance of the significant negative correlation gradually transformed into a significant positive correlation with the increasing of the wavelength. At 750 nm to 1 350 nm band, the correlation coefficient between canopy spectral reflectance and the original above-ground dry biomass of summer maize was 0.578 to 0.733. All selected bands of vegetation index from Tab. 1 are within 430 nm to 720 nm and 750 nm to 1350 nm that were included in stable band platform of correlation coefficient.

2.4 Construction of above-ground dry biomass spectrum monitoring model of corn

Above-ground dry biomass and corresponding vegetation index (n = 240, 5 gradient nitrogen species, 4 gradients phosphate, 3 repeat and 2 years of experiments) were selected in this experiment from the year of 2011 to 2013 of summer maize and established the monitoring model based on different growth stages (Tab. 3). 21 vegetation index and liner, logarithmic, quadratic and exponential equation were chosen to establish fittingregression model, and analyzed the fitting precision variation(R^2 and F value) about above-ground dry biomass model. Four models which based on a same vegetation index, that the parabolic model generally had a higher determination coefficient, the linear, logarithmic and exponential fitting model had a similar determination coefficient and the equation parameters.

For the choice of crop physiological ecology parameter of estimation model, not only required high determination coefficient and F value of regression model, but also repeatability. From Tab. 3, three fitting models with determination coefficient and F values from each of the growth stages were analysed precision inspection (Tab. 4). All above-ground dry biomass determination coefficient of fitting models were lower due to the little LAI and the interference of soil background at the huge bellbottom stage of summer maize. At silking stage, both determination coefficient of regression mode and F values were improved, and above-ground dry biomass and vegetation index PSSRc and MTCI had a higher model determination coefficient. At filling stage, there were higher determination coefficients of model which structured by above-ground dry biomass and vegetation index GNDVI and NDVI4, so the model was chosen as the more suitable model for the further accuracy test. At maturity, established model with above-ground dry biomass and vegetation index DI had the highest determination coefficient and higher F value.

Tab. 3 Parameters of regression models between ADMA and vegetation index of summer maize at different growth stages

Vegetation Index	Regression Model	Huge bellbottom stage		Silking stage		Filling stage		Maturity stage	
		R^2	F	R^2	F	R^2	F	R^2	F
GI	Linear	0.098	0.655	0.041	0.254	0.244	1.932	0.281	2.350
	Logarithm	0.099	0.658	0.037	0.229	0.251	2.011	0.278	2.312
	Quadratic	0.099	0.276	0.143	0.419	0.270	0.924	0.318	1.164
	Exponential	0.110	0.738	0.041	0.254	0.222	1.714	0.297	2.535
PSSRa	Linear	0.688	13.234	0.453	4.965	0.323	2.861	0.491	5.799
	Logarithm	0.697	13.795	0.551	7.377	0.366	3.459	0.502	6.056
	Quadratic	0.734	6.892	0.716	17.179	0.424	1.843	0.541	2.942
	Exponential	0.666	11.955	0.461	5.141	0.345	3.158	0.477	5.469
PSSRb	Linear	0.548	7.285	0.536	6.942	0.434	4.608	0.768	19.850
	Logarithm	0.611	9.433	0.640	10.682	0.500	5.997	0.777	20.906
	Quadratic	0.849	26.292	0.840	28.879	0.583	3.501	0.784	9.089
	Exponential	0.545	7.180	0.544	7.172	0.453	4.974	0.759	18.888
PSSRc	Linear	0.616	9.628	0.449	4.890	0.345	3.164	0.532	6.809
	Logarithm	0.642	10.761	0.557	7.546	0.390	3.842	0.544	7.169
	Quadratic	0.749	7.452	0.857	35.487	0.439	1.954	0.582	3.477
	Exponential	0.601	9.055	0.457	5.056	0.369	3.506	0.505	6.125
SRPI	Linear	0.192	1.427	0.001	0.007	0.004	0.024	0.114	0.771
	Logarithm	0.186	1.375	0.002	0.010	0.003	0.021	0.114	0.772
	Quadratic	0.315	1.152	0.554	3.104	0.181	0.554	0.114	0.321
	Exponential	0.194	1.440	0.003	0.016	0.002	0.015	0.091	0.603
DI	Linear	0.675	12.446	0.666	11.957	0.755	18.469	0.884	45.590
	Logarithm	0.707	14.466	0.699	13.921	0.771	20.163	0.891	49.008
	Quadratic	0.766	71.332	0.806	10.354	0.797	9.829	0.897	26.184
	Exponential	0.673	12.359	0.684	12.982	0.772	20.290	0.887	47.284
DVI	Linear	0.791	22.669	0.617	9.653	0.514	6.345	0.840	31.549
	Logarithm	0.800	24.072	0.645	10.908	0.529	6.736	0.844	32.501
	Quadratic	0.802	20.788	0.811	10.732	0.585	3.525	0.858	15.145
	Exponential	0.857	37.169	0.634	10.405	0.536	6.927	0.840	31.532
DD	Linear	0.805	24.808	0.767	19.709	0.704	14.250	0.726	15.881
	Logarithm	0.811	25.676	0.725	15.800	0.624	9.950	0.748	17.798
	Quadratic	0.815	11.006	0.767	8.213	0.708	6.049	0.761	7.962
	Exponential	0.814	26.270	0.792	22.856	0.714	15.008	0.750	18.015
MTCI	Linear	0.721	15.498	0.802	24.316	0.657	11.493	0.663	11.798
	Logarithm	0.769	19.935	0.781	21.441	0.652	11.253	0.717	15.202
	Quadratic	0.804	10.271	0.802	10.137	0.663	4.927	0.797	9.793
	Exponential	0.724	15.757	0.863	27.840	0.660	11.649	0.683	12.955
GNDVI	Linear	0.589	8.591	0.710	14.668	0.791	22.726	0.861	37.211
	Logarithm	0.626	10.060	0.740	17.052	0.799	23.810	0.871	40.531
	Quadratic	0.851	38.799	0.840	13.144	0.806	10.404	0.878	27.135
	Exponential	0.591	8.659	0.725	15.833	0.809	25.488	0.861	37.125
NPCI	Linear	0.187	1.378	0.002	0.010	0.003	0.021	0.114	0.772
	Logarithm	0.242	1.920	0.020	0.123	0.015	0.090	0.134	0.929
	Quadratic	0.315	1.149	0.557	3.137	0.178	0.541	0.114	0.323
	Exponential	0.189	1.395	0.003	0.021	0.002	0.012	0.091	0.603
NPQI	Linear	0.100	0.670	0.012	0.071	0.311	2.702	0.025	0.156
	Logarithm	—	—	—	—	—	—	—	—
	Quadratic	0.477	2.278	0.222	0.713	0.436	1.929	0.027	0.070
	Exponential	0.088	0.578	0.013	0.076	0.302	2.600	0.031	0.191
PRI	Linear	0.337	3.046	0.700	13.999	0.219	1.682	0.031	0.190
	Logarithm	0.384	3.733	0.714	14.968	0.259	2.092	0.020	0.121
	Quadratic	0.430	1.885	0.723	6.529	0.258	0.868	0.236	0.773
	Exponential	0.377	3.626	0.672	12.310	0.239	1.889	0.025	0.151

Tab. 3

Vegetation Index	Regression Model	Huge bellbottom stage		Silking stage		Filling stage		Maturity stage	
		R^2	F	R^2	F	R^2	F	R^2	F
SIPI	Linear	0.013	0.081	0.185	1.363	0.006	0.034	0.094	0.625
	Logarithm	0.014	0.082	0.184	1.357	0.006	0.033	0.094	0.621
	Quadratic	0.013	0.081	0.186	1.368	0.006	0.035	0.095	0.628
	Exponential	0.018	0.109	0.205	1.546	0.007	0.043	0.075	0.490
MSR705	Linear	0.760	19.001	0.794	23.154	0.769	19.963	0.528	6.703
	Logarithm	0.761	19.076	0.765	19.577	0.753	18.299	0.576	8.145
	Quadratic	0.762	7.992	0.804	10.266	0.770	8.391	0.676	5.217
	Exponential	0.762	19.261	0.817	26.798	0.762	19.160	0.556	7.499
PSRI	Linear	0.192	1.426	0.780	21.283	0.381	3.694	0.485	5.649
	Logarithm	—	—	—	—	—	—	—	—
	Quadratic	0.237	0.777	0.784	9.075	0.405	1.705	0.848	13.936
	Exponential	0.198	1.481	0.804	24.580	0.386	3.771	0.478	5.492
RGR	Linear	0.040	0.247	0.301	2.587	0.042	0.261	0.111	0.746
	Logarithm	0.039	0.241	0.301	2.586	0.040	0.251	0.111	0.752
	Quadratic	0.064	0.172	0.301	1.078	0.069	0.185	0.123	0.350
	Exponential	0.046	0.287	0.298	2.553	0.033	0.202	0.118	0.802
NDVI1	Linear	0.824	28.164	0.766	19.660	0.627	10.086	0.779	21.134
	Logarithm	0.837	30.921	0.769	19.934	0.617	9.658	0.790	22.522
	Quadratic	0.853	14.454	0.773	8.491	0.627	4.203	0.805	10.321
	Exponential	0.830	29.197	0.790	22.535	0.643	10.803	0.796	23.456
NDVI2	Linear	0.621	9.830	0.720	15.458	0.622	9.882	0.839	31.335
	Logarithm	0.644	10.849	0.743	17.379	0.626	10.028	0.842	32.016
	Quadratic	0.805	13.935	0.835	12.671	0.629	4.241	0.848	13.898
	Exponential	0.619	9.764	0.735	16.642	0.645	10.899	0.839	31.270
NDVI3	Linear	0.699	13.903	0.618	9.703	0.378	3.652	0.526	6.648
	Logarithm	0.701	14.060	0.640	10.662	0.385	3.757	0.529	6.749
	Quadratic	0.699	13.903	0.843	13.395	0.400	1.664	0.574	3.363
	Exponential	0.677	12.564	0.630	10.218	0.405	4.086	0.514	6.347
NDVI4	Linear	0.590	8.619	0.711	14.753	0.796	23.369	0.856	35.791
	Logarithm	0.627	10.079	0.741	17.126	0.802	24.379	0.867	39.026
	Quadratic	0.850	47.507	0.839	13.003	0.809	10.599	0.870	27.117
	Exponential	0.591	8.677	0.726	15.929	0.814	26.237	0.856	35.691

Note:—denotes arguments (NPQI, NPQI) comprises a non-positive value, which can not be calculated power function model.

2.5 Precision verification of maize above-ground dry biomass spectrum monitoring

To test the stability and reliability of the monitoring model, root-mean-square error (RMSE) and relative error (RE) of summer corn were verified and tested at different growth stages according to the independent experimental data ($n=240$) from 2011 to 2014 year. Chose 3 determination coefficient and a model with higher F value higher from each stages tested the precision verification about above-ground dry biomass model, and selected a most suitable model which has a better stability and repeatability with lower RMSE and RE. The results show that the model established between above-ground dry biomass and vegetation index (GNDVI, PSSRc, NDVI4 and DI) were the most suitable model.

3 Discussion

In order to study the above-ground dry matter, fresh crop leaves are sampled and weighted in traditional methods which were not only time-consuming and laborious, but also destructive to the crops. However, remote sensing technology can be used to collect and process the field information of crop canopy rapidly and effectively without any destruction, then a large area of crops can be detected quickly and accurately.

The existing researches focus on fitting model of above-ground dry matter on maturity stage[32-33], and the corresponding researches on crop growth period are less. A fitting model, in this experiment, was

established between vegetation index which structured by a variety of bands and different stages of summer maize and above-ground dry matter, and the corresponding precision was tested at the same time. Except that, we analyzed the relationship between above-ground dry matter and canopy reflectance spectra at the point of view of statistics, and established the corresponding monitoring model. Finally, it provides a quantitative index for monitoring and diagnosing field corn growth.

Tab. 4 Verification of regression models between ADMA and vegetation index of summer maize at different growth stages

Growth stage	Vegetation index	Fitting model	Root mean square deviation/(t·hm^{-2})	Relative error/%
Huge bellbottom stage	DVI	$y = 1.164e^{0.336x}$	2.096	10.85
	GNDVI	$y = -190.298 + 659x - 520.752x^2$	0.945	5.53
	NDVI1	$y = -29.000 + 149.782x - 116.928x^2$	1.644	9.23
Silking stage	PSSRc	$y = -20.977 + 9.796x - 0.501x^2$	1.044	3.93
	MTCI	$y = 14.834e^{0.007x}$	2.246	7.54
	NDVI3	$y = -367.796 + 976.526x - 605.895x^2$	1.994	7.52
Filling stage	GNDVI	$y = 16.183e^{0.081x}$	5.473	10.57
	NDVI4	$y = -41.278 + 238.043x - 148.690x^2$	5.013	11.05
	NDVI4	$y = 16.104e^{0.082x}$	5.408	10.47
Maturity stage	DI	$y = 130.535 + 68.978\ln x$	2.175	4.932
	DI	$y = -276.451 + 1\,979.524x - 2\,982.515x^2$	2.234	5.516
	DI	$y = 11.254e^{5.312x}$	1.761	4.578

Compared to the wide band vegetation index, however, the vegetation index of the narrow band is easy susceptible to the effects of instruments, environmental noise and background that may be the important reason for the difference which can be decreased by vegetation index of band combination in the result of research, and improve the accuracy of the model according to the experiment results[34-36].

Seven models which contained 800 nm and 550 nm parameters were selected from 12 models (Tab. 4) in different growth stages. In many statements, 800 nm and 550 nm band parameters has been applied to the large number of vegetation indexes and a variety of plant growth monitoring, relatively speaking, the research on growth monitoring of summer maize in different growth period is less. In this paper, the correlation analysis between the above-ground biomass of summer maize and various spectral vegetation indexes at different stages have been carried out, so as to the verification of relevant models. The results showed that the sensitive bands appeared some differences in summer corn at different growth stages which result in different choices of vegetation index. Otherwise, DI has a higher determination coefficient and F value, and all have smaller root mean square error and relative error in the later stages when biomass become higher.

Nine models have been selected from growth former medium-term (huge bellbottom stage, silking stage and filling stage), the models with NDVI and GNDVI parameter of model vegetation index were 4 and 2 respectively, these two kings of models have been widely used to the construction of nitrogen, LAI and biomass model. Yet, at the maturity stage, DI vegetation index better solves the problem of drawback, easy saturation, in NDVI formula[28,37].

In this study, the establishment of the optimality model at the maturity stage to above-ground dry biomass were based on vegetation index (DI) of the exponential function model, which with the similar conclusions compared to the previous studies[38-39], and other DI in this growth period to verify the model also has relatively low root mean square error and relative error. Models were established according to vegetation index (DI) with good stability and high precision. It is particularly important that build a maturity stage model what has high practical significance for the fact of that existing on above-ground dry biomass research focus on the maturity stage, and mature stage dry matter quality research has important application value.

This experiment was based on the fitting analysis of spectral vegetation index about above-ground dry biomass of summer maize at different stage is, the optimum vegetation index has bigger difference, so it can not be used to monitor all growth stages of

vegetation index so far. The model for the quality of dry matter in the spectrum monitoring of the general suitable for all growth stages is still needed to be further studied.

4 Conclusion

(1) There were significant differences between above-ground dry biomass and total nitrogen under different conditions of fertilizer. At different growth stages, total nitrogen was decreased while above-ground dry biomass was increased gradually. It has a strong correlation between canopy spectral reflectance, total nitrogen and above-ground dry biomass.

(2) At the huge bellbottom stage, silking stage, filling stage and maturity stage of summer maize, the optimal prediction model of ground dry biomass were: $y = -190.298 + 659x - 520.752x^2$ (GNDVI), $y = -20.977 + 9.796x - 0.501x^2$ (PSSRc), $y = 16.104e^{0.082x}$ (NDVI4) and $y = 6.344e^{0.239x}$ (DI).

References

[1] ZHAO Yingshi. Remote sensing application principles and methods[M]. Beijing: Science Press, 2003. (in Chinese)

[2] ZHANG Liangpei, ZHENG Lanfen, TONG Qingxi. The estimation of vegetation variables based on high resolution spectra[J]. Journal of Remote Sensing, 1997,1(2):110 -114. (in Chinese)

[3] WANG Yuan, WANG Fumin, HUANG Jingfeng. The models for estimation of dry biomass from different components of rapeseed using canopy spectral data[J]. Acta Agriculturae Zhejiangensis, 2004,16(2):79 -83. (in Chinese)

[4] SHIBAYAMA M, AKIYAMA T. Seasonal visible nearinfrared and midinfrared spectra of rice canopies in relation to LAI and above-ground dry biomass[J]. Remote Sensing of Environment,1989,27(2):119 -197.

[5] SONG Kaishan, ZHANG Bai, LI Fang, et al. Correlative analyses of hyperspectral reflectance, soybean LAI and aboveground biomass [J]. Transactions of the CSAE, 2005,21(1):36 -40. (in Chinese)

[6] ZHUANG Dongying, LI Weiguo, WU Liquan. Estimating winter wheat biomass based on satellite remote sensing [J]. Journal of Arid Land Resources and Environment, 2013,27(10): 158 -162. (in Chinese)

[7] CHU Duo, DEJI Yangzong, PUBU Ciren, et al. Aboveground biomass in the north Tibet and estimate model using remote sensing data[J]. Journal of Natural Resource, 2013,28(11): 2000 -2011. (in Chinese)

[8] FU Yuanyuan, WANG Jihua, YANG Guijun, et al. Band depth analysis and partial least square regression based winter wheat biomass estimation using hyperspectral measurements[J]. Spectroscopy and Spectral Analysis, 2013,33(5):1315 -1319. (in Chinese)

[9] TOMPPO E, NILSSON M, ROSENGREN M. Simultaneous use of landsat-TM and IRS -1C WiFS data in estimating large area tree stem volume and aboveground biomass[J]. Remote Sensing of Environment, 2002, 82 (1):156 -171.

[10] SPANNER M, JOHNSON L, MILLER J, et al. Remote sensing of seasonal leaf-area index across the oregon transect [J]. Ecological Applications, 1994, 4(2): 258 -271.

[11] YANG Y H, FANG J Y, PAN Y D, et al. Aboveground biomass in Tibetan grasslands [J]. Journal of Arid Environments, 2009, 73(1): 91 -95.

[12] CHOUDHURY B J. Relationships between vegetation indices, radiation absorption and net photosynthesis evaluated by a sensitivity analysis [J]. Remoting Sensing Environment, 1987, 22(2): 209 -233.

[13] SMITH R C G, ADAMS J, STEPHENS D J, et al. Forecasting wheat yield in a mediterranean-type environment from the NOAA satellite [J]. Australian Journal of Agricultural Research, 1995, 46(1): 113 -125.

[14] BLACKBURN G A. Quantifying chlorophylls and carotenoids at leaf and canopy scales: an evaluationof some hyperspectral approaches[J]. Remote Sensing of Environment, 1998,66(3):273 -285.

[15] PENUELAS J, GAMON J A, FREDEEN A L, et al. Reflectance indices associated with physiological changes in nitrogen-limited and water-limited sunflower leaves [J]. Remote Sensing of Environment, 1994, 48(2): 135 -146.

[16] BUSCHMAN C, NAGEL E. In vivo spectroscopy and internal optics of leaves as a basis for remote sensing of vegetation[J]. International Journal of Remote Sensing, 1993,14(4):711 -722.

[17] JORDAN C F. Derivation of leaf area index from quality of light on the forest floor[J]. Ecology, 1969,50(4): 663 -666.

[18] LE MAIRE G, FRANçOIS C, DUFRENE E. Towards universal broad leaf chlorophyll indices using PROSPECT simulated database and hyperspectral reflectance measurements [J]. Remote Sensing of Environment, 2004,89(1):1 -28.

[19] DASH J, CURRAN P J. The MERIS terrestrial chlorophyll index[J]. International Journal of Remote Sensing, 2004, 25(23):5403 -5413.

[20] DAUGHTRY C S T, WALTHALL C L, KIM M S, et al. Estimating corn leaf chlorophyll concentration from leaf and canopy reflectance[J]. Remote Sensing of Environment, 2000,74(2):229-239.

[21] PENUELAS J, BARET F, FILELLA I. Semi-empirical indices to assess carotenoids/chlorophyll a ratio from leaf spectral reflectance[J]. Photosynthetica, 1995,31:221-230.

[22] BARNES J D, BALAGUER L, MANRIQUE E, et al. A reappraisal of the use of DMSO for the extraction and determination of chlorophylls-a and chlorophylls-b in lichens and higher plants[J]. Environmental and Experimental Botany, 1992,32(2):85-100.

[23] GAMON J A, PENUELAS J, FIELD C B. A narrow-waveband spectral index that tracks diurnal changes in photosynthetic efficiency[J]. Remote Sensing of Environment, 1992, 41(1):35-44.

[24] SIMS D A, GAMON J A. Relationships between leaf pigment content and spectral reflectance across a wide range of species, leaf structures and developmental stages[J]. Remote Sensing of Environment, 2002,81(2-3): 337-354.

[25] STEDDOM K, HEIDEL G, JONES D, et al. Remote detection of rhizomania in sugar beets[J]. Phytopathology, 2003,93(6):720-726.

[26] MA B L, MORRISON M J, DWYER L M. Canopy light reflectance and field greenness to assess nitrogen fertilization and yield of maize[J]. Agronomy Journal, 1996,88(6):915-920.

[27] SERRANO L, FILELLA I, PENUELAS J. Remote sensing of biomass and yield of winter wheat under different nitrogen supplies[J]. Crop Science, 2000,40(3):723-731.

[28] GITELSON A A, KAUFMAN Y J, MERZLYAK M N. Use of a green channel in remote sensing of global vegetation from EOS-MODIS[J]. Remote Sensing of Environment, 1996,58(3):289-298.

[29] SHEN Lixia, WANG Pu, ZHANG Ruanbin. Effect of nitrogen supply on yield and grain filling in summer maize with different crop density[J]. Plant Nutrition and Fetilizer Science, 2005,11(3):314-319. (in Chinese)

[30] DANG Hongkai, LI Wei, CAO Caiyun, et al. Effect of late milk irrigation on water use efficiency and dry matter distribution of maize[J]. Transactions of the Chinese Society for Agricultural Machinery, 2014,45(5): 131-138. (in Chinese)

[31] AL ABBAS A H, BARR R, HALL J D. Spectra of normal and nutrient-deficient maize leaves[J]. Agronomy Journal, 1974,66(1): 16-20.

[32] QI J, CABOT F, MORAN M S, et al. Biophysical parameter estimations using multidirectional spectral measurements[J]. Remote Sensing of Environment, 1995,54(1):71-83.

[33] JACQUEMOUD S, BACOUR C, POILVE H, et al. Comparison of four radiative transfer models to simulate plant canopies reflectance: direct and inverse mode[J]. Remote Sensing of Environment, 2000,74(3):471-481.

[34] DENTE L, SATALINO G, MATTIA F, et al. Assimilation of leaf area index derived from ASAR and MERIS data into CERES-Wheat model to map wheat yield[J]. Remote Sensing of Environment, 2008, 112(4): 1395-1407.

[35] WIT A D, DUVEILLER G, DEFOURNY P. Estimating regional winter wheat yield with WOFOST through the assimilation of green area index retrieved from MODIS observations[J]. Agricultural and Forest Meteorology, 2012, 164(6): 39-52.

[36] MANGIAROTTI S, MAZZEGA P, JARLAN L, et al. Evolutionary bi-objective optimization of a semi-arid vegetation dynamics model with NDVI and σ_0 satellite data[J]. Remote Sensing of Environment, 2008, 112(4): 1365-1380.

[37] TANG Y L, WANG R C, HUANG J F. Relations between red edge characteristics and agronomic parameters of crops[J]. Pedosphere, 2004,14(4):467-474.

[38] RAUSTE Y. Multi-temporal JERS SAR data in boreal forest biomass mapping[J]. Remote Sensing of Environment, 2005,97(2): 263-275.

[39] LUCAS R M, CRONIN N, LEE A, et al. Empirical relationships between AIRSAR backscatter and LiDAR-derived forest biomass, Queensland, Australia[J]. Remote Sensing of Environment, 2006,100(3):407-425.

doi:10.6041/j.issn.1000-1298.2016.03.036

基于高光谱植被指数的夏玉米地上干物质量估算模型研究

刘冰峰[1]　李　军[1]　贺　佳[2]　师祖姣[1]

(1.西北农林科技大学农学院,陕西杨凌 712100;2.河南省农业科学院农业经济与信息研究所,郑州 450002)

摘要:2011—2014 年连续实施夏玉米长势监测定位实验,在 5 种不同施氮量、4 种不同施磷量和 2 个夏玉米品种处理下,测定了大喇叭口期、吐丝期、灌浆期和成熟期夏玉米冠层高光谱反射率及对应的地上干物质积累量(Above-ground dry matter accumulation, ADMA)。选取了 21 个光谱植被指数,利用 2011 年和 2013 年综合数据进行线性函数、对数函数、二次函数和指数函数模型拟合。在每个生育时期,选择决定系数和 F 值最高的 3 个模型,并用 2012 年和 2014 年测定光谱数据与地上干物质量对拟合模型进行均方根差和相对误差的验证,选择均方根差和相对误差较小的拟合模型为最适模型。结果表明,在大喇叭口期、吐丝期、灌浆期和成熟期,夏玉米地上干物质量的最佳拟合光谱植被指数分别为 GNDVI、PSSRc、NDVI4 和 DI。

关键词:夏玉米;冠层;地上干物质量;高光谱植被指数;估算模型

中图分类号:S127　　**文献标识码**:A　　**文章编号**:1000-1298(2016)03-0254-09

Estimation Models of Above-ground Dry Matter Accumulation of Summer Maize Based on Hyperspectral Remote Sensing Vegetation Indexes

Liu Bingfeng[1]　Li Jun[1]　He Jia[2]　Shi Zujiao[1]

(1. *College of Agronomy, Northwest A&F University, Yangling, Shaanxi* 712100, *China*

2. *Agricultural Economy and Information Research Institution, Henan Academy of Agricultural Sciences, Zhengzhou* 450002, *China*)

Abstract: An on-site field experiment, which includes five nitrogen fertilizer application rate treatments, four phosphorus fertilizer application rate treatments and two summer maize cultivars treatments, was conducted at agricultural experimental station of Northwest A&F University during 2011—2014. Summer maize canopy spectral reflectance and above-ground dry matter accumulation (ADMA) were measured at the huge bellbottom stage, silking stage, filling stage and maturity stage of summer maize. 21 canopy vegetation indexes of hyperspectral remote sensing in 2011 and 2013 were chosen to establish liner, logarithmic, quadratic and exponential regression relationship between ADMA and canopy spectral parameters for each cultivar. Different regression models were applied to establish the relationship between spectrum vegetation indexes and summer maize ADMA. Three models with high coefficients and F values at each growth stage were chosen to verify root mean square error and relative error with data of canopy spectral reflectance and ADMA in 2012 and 2014 separately. The smallest root mean square error and relative error models were chosen as the best models for estimation ADMA of maize. The results show that, at the huge bellbottom stage, filling stage and maturity stage of maize, spectrum vegetation indexes for the best fitting regression relationship models with ADMA were GNDVI, PSSRc, NDVI4 and DI. These models could be used as the best models for the estimation of summer maize above-ground ADMA.

Key words: summer maize; canopy; above-ground dry matter accumulation; hyperspectral remote sensing vegetation indexes; estimation model

收稿日期:2015-09-08　修回日期:2015-12-18

基金项目:国家高技术研究发展计划(863 计划)项目(2013AA102902)和国家自然科学基金项目(31571620、31071374)

作者简介:刘冰峰(1987—),男,博士生,主要从事作物遥感监测研究,E-mail:lbf@nwsuaf.edu.cn

通信作者:李军(1964—),男,教授,博士生导师,主要从事旱作农业生态、高效农作制度和数字农作技术研究,E-mail:junli@nwsuaf.edu.cn

引言

作物冠层光谱分析是一种无损测试遥感技术，利用高光谱技术可监测作物物理和化学参数，对高光谱遥感数据进行线性和非线性组合构成植被指数，可用于指示植被长势、光合物质积累量等信息[1]。

作物生育期间地上干物质积累量（Above-ground dry matter accumulation，ADMA）是作物产量形成的基础，通过高光谱遥感植被指数反演作物干物质积累量，可以实现遥感对作物生长状况动态监测和产量反演。张良培等[2]利用归一化植被指数（NDVI）建立了鄱阳湖地区的地上生物量模型。王渊等[3]利用油菜的各组分生物量（叶、茎秆质量和荚果质量）分别与比值植被指数（RVI）、NDVI 建立了回归模型。SHIBAYAMA 等[4]采用比值指数（R_{1100}/R_{1200}）较好地预测模拟了双季稻的干物质量。宋开山等[5]研究表明，RVI（R_{760}/R_{710}）可以模拟反演大豆地上鲜物质积累量。庄东英等[6]基于冬小麦生物量模型（WBM）研究表明，利用卫星影像的 NDVI 转换模型，可较好模拟冬小麦生物量，并能大面积准确获取不同等级生物量的长势信息。除多等[7]、付元元等[8]研究指出，多种植被指数模型均可估算青藏地区草地地上生物量。但以上研究均基于较低生物量条件下的光谱模拟估算生物量，在较高生物量条件下，光谱模型存在饱和问题，降低了模型的适用性[9-12]。

综上所述，众多学者利用多种植被指数模拟预测植被的地上生物量信息，并取得了可观的研究成果。但关于光谱模型估算较高生物量的研究相对较少，利用光谱估算夏玉米地上生物量的研究也相对较少。本文通过高光谱不同波段组合植被指数和归一化差值植被指数，预测模拟夏玉米地上干物质量，同时建立并验证基于植被指数的夏玉米地上干物质量回归模型，以期为高光谱遥感监测夏玉米长势监测提供依据，为光谱植被指数估算较高生物量提供理论基础。

1　材料与方法

1.1　实验设计

于 2011—2014 年在西北农林科技大学北校区农作一站（34°29′N，108°06′E），设置不同氮磷营养水平和品种的夏玉米长势进行高光谱遥感监测田间实验。实验地区气候为暖温带半湿润气候，海拔高度 400 m 左右，供试土壤为红油土，质地为粉砂粘壤土，0 ~ 20 cm 土层养分含量分别为：有机质质量比 10.48 mg/kg、全氮质量比 1.20 g/kg、碱解氮质量比 36.48 mg/kg、速效磷质量比 12.49 mg/kg。采取二次裂区设计，氮肥为主处理，磷肥为副处理，品种为副副处理，并实行多年连续定位施肥处理。实验设置 5 个氮肥处理 N0、N1、N2、N3、N4，对应施氮量分别为 0、75、150、225、300 kg/hm^2（纯氮），总氮肥 60% 作为基肥，40% 作为追肥。设置 4 个磷肥处理 P0、P1、P2、P3，对应施磷量分别为 0、60、120、180 kg/hm^2（P_2O_5），磷肥作为底肥一次性施入。2 个供试夏玉米品种分别为豫玉 22（平展型）和郑单 958（紧凑型），种植密度：豫玉 22 为 5.25 × 10^{4}株/hm^2，郑单 958 为 6.75 × 10^{4}株/hm^2。

1.2　测定指标及方法

1.2.1　冠层光谱反射率测定

在夏玉米大喇叭口期（7 月 15 日）、吐丝期（8 月 2 日）、灌浆期（8 月 17 日）和乳熟期（9 月 10 日），选择晴朗无云、无风天气，用 ASD FieldSpec3 高光谱仪，在 10:30—13:30 测定冠层光谱反射率。光谱采样每个小区设 3 次重复，每次重复 10 个为一组，以其平均值作为该小区冠层光谱反射率。

1.2.2　地上干物质量测定与全氮含量测定

田间光谱测量后，立即剪取测定区域地上夏玉米鲜生物量并带回实验室，进行杀青和干燥处理，并于干燥后称量。采用凯氏定氮仪进行全氮含量的测定。

1.3　高光谱遥感估算模型的建立及精度检验

拟合模型包括：简单线性函数 $y = c + ax$；对数函数 $y = c + a\ln x$；二次函数 $y = c + ax + bx^2$；指数函数 $y = ce^{ax}$。以上模型中，y 为地上干物质量拟合值，x 为光谱变量，c 为常数，a、b 为方程参数。

由单变量和多变量回归模型估计出的参数，其精度可用均方根差（RMSE）和相对误差（RE）来评价。

$$V_{\mathrm{RMSE}} = \sqrt{\sum_{i=1}^{n} (y_i - \hat{y}_i)^2 / n}$$

$$V_{\mathrm{RE}} = (y_i - \hat{y}_i) / y_i \times 100\%$$

式中　y_i——实测值　　$\hat{y}_i$——预测值

n——样本数　　V_{RMSE}——均方根差

V_{RE}——相对误差

1.4　植被指数的选择

在已有研究成果基础上，选取 21 种比值植被指数及归一化植被指数（表 1）建立夏玉米地上干物质量高光谱遥感监测模型。

2　结果与分析

2.1　不同氮磷水平对夏玉米各生育时期地上干物质量的影响

以 2011 年和 2013 年大田夏玉米实验数据平均值为例，分析了不同施肥处理下各生育时期地上干物质量和全氮含量变化动态，如表 2 所示。从大喇

表 1 本文采用的高光谱植被指数

Tab. 1 Hyperspectral vegetation indices used in this study

植被指数	计算公式	文献序号
绿度指数（GI）	$R = R_{554}/R_{677}$	[13]
特征色素简单比值指数 a（PSSRa）	$R = R_{800}/R_{680}$	[14]
特征色素简单比值指数 b（PSSRb）	$R = R_{800}/R_{635}$	[14]
特征色素简单比值指数 c（PSSRc）	$R = R_{800}/R_{470}$	[14]
简单色素比值指数（SRPI）	$R = R_{430}/R_{680}$	[15]
差值指数（DI）	$R = R_{800} - R_{550}$	[16]
差值植被指数（DVI）	$R = R_{800} - R_{680}$	[17]
双差指数（DD）	$R = R_{750} - R_{720} - (R_{700} - R_{670})$	[18]
中分辨率陆地叶绿素成像指数（MTCI）	$R = (R_{750} - R_{710})/(R_{710} - R_{680})$	[19]
绿色归一化植被指数（GNDVI）	$R = (R_{801} - R_{550})/(R_{800} + R_{550})$	[20]
叶绿素归一化植被指数（NPCI）	$R = (R_{680} - R_{430})/(R_{680} + R_{430})$	[21]
归一化脱镁作用指数（NPQI）	$R = (R_{415} - R_{435})/(R_{415} + R_{435})$	[22]
光化学植被指数（PRI）	$R = (R_{531} - R_{570})/(R_{530} + R_{570})$	[23]
结构加强色素指数（SIPI）	$R = (R_{800} - R_{445})/(R_{800} - R_{680})$	[21]
改进红边比值植被指数（MSR705）	$R = (R_{750} - R_{445})/(R_{705} - R_{445})$	[24]
植物衰老指数（PSRI）	$R = (R_{680} - R_{500})/R_{750}$	[24]
红绿比值指数（RGR）	$R = (R_{612} + R_{660})/(R_{510} + R_{560})$	[25]
归一化植被指数 1（NDVI1）	$R = (R_{760} - R_{708})/(R_{760} + R_{708})$	[25]
归一化植被指数 2（NDVI2）	$R = (R_{800} - R_{600})/(R_{800} + R_{600})$	[26]
归一化植被指数 3（NDVI3）	$R = (R_{900} - R_{680})/(R_{900} + R_{680})$	[27]
归一化植被指数 4（NDVI4）	$R = (R_{780} - R_{550})/(R_{780} + R_{550})$	[28]

注：R_{554} 表示 554 nm 波长的光谱反射率，其余类推。

表 2 不同施肥量处理下各生育时期夏玉米地上干物质量与冠层全氮质量分数

Tab. 2 ADMA and total nitrogen content of canopy under different fertilization treatments at different growth stages of maize

施肥处理		大喇叭口期		吐丝期		灌浆期		成熟期	
		干物质量/（t·hm^{-2}）	全氮质量分数/%	干物质量/（t·hm^{-2}）	全氮质量分数/%	干物质量/（t·hm^{-2}）	全氮质量分数/%	干物质量/（t·hm^{-2}）	全氮质量分数/%
P0	N0	11.64^{d}	1.13^{c}	18.38^{d}	1.04^{b}	32.54^{d}	0.96^{c}	37.90^{c}	0.84^{d}
	N1	13.09^{c}	1.34^{b}	21.09^{c}	1.39^{a}	35.14^{c}	1.08^{b}	41.68^{b}	0.90^{cd}
	N2	13.79^{b}	1.36^{b}	21.32^{b}	1.41^{a}	35.81^{c}	1.07^{b}	42.13^{b}	1.00^{bc}
	N3	13.78^{b}	1.41^{b}	21.65^{a}	1.48^{a}	40.48^{b}	1.25^{a}	42.35^{b}	1.12^{ab}
	N4	16.35^{a}	1.69^{a}	22.12^{a}	1.53^{a}	42.93^{a}	1.31^{a}	44.42^{a}	1.24^{a}
P1	N0	12.14^{d}	1.27^{d}	19.01^{e}	1.26^{c}	36.20^{d}	1.17^{c}	39.65^{c}	1.18^{c}
	N1	14.10^{c}	1.50^{bc}	20.92^{d}	1.44^{b}	36.15^{d}	1.19^{c}	43.18^{be}	1.27^{b}
	N2	14.07^{c}	1.46^{c}	21.20^{c}	1.43^{b}	40.64^{c}	1.36^{b}	44.04^{b}	1.26^{b}
	N3	14.96^{b}	1.58^{b}	21.92^{b}	1.58^{a}	41.79^{b}	1.39^{ab}	46.63^{a}	1.39^{a}
	N4	17.04^{a}	1.81^{a}	22.50^{a}	1.63^{a}	45.74^{a}	1.51^{a}	46.87^{a}	1.41^{a}
P2	N0	12.55^{d}	1.47^{d}	19.74^{d}	1.49^{c}	37.84^{d}	1.31^{c}	40.86^{d}	1.24^{b}
	N1	14.46^{c}	1.64^{c}	20.04^{d}	1.50^{c}	40.18^{c}	1.45^{b}	43.11^{c}	1.34^{ab}
	N2	15.19^{c}	1.80^{b}	24.19^{c}	1.83^{b}	48.08^{b}	1.72^{a}	48.86^{b}	1.44^{a}
	N3	17.11^{b}	1.96^{a}	25.26^{b}	1.87^{b}	47.73^{b}	1.70^{a}	48.61^{b}	1.47^{a}
	N4	17.93^{a}	2.07^{a}	26.44^{a}	1.97^{a}	50.66^{a}	1.76^{a}	51.60^{a}	1.52^{a}
P3	N0	12.70^{e}	1.69^{e}	20.96^{d}	1.69^{b}	40.55^{d}	1.35^{d}	40.99^{e}	1.27^{c}
	N1	14.37^{d}	1.85^{d}	21.41^{c}	1.69^{b}	41.69^{c}	1.62^{c}	44.36^{d}	1.47^{b}
	N2	15.63^{c}	2.01^{c}	25.00^{b}	1.99^{a}	45.32^{b}	1.68^{bc}	47.31^{c}	1.56^{ab}
	N3	17.27^{b}	2.16^{b}	25.44^{b}	2.03^{a}	45.38^{b}	1.77^{b}	49.57^{b}	1.71^{a}
	N4	18.77^{a}	2.37^{a}	26.72^{a}	2.13^{a}	51.11^{a}	1.97^{a}	54.02^{a}	1.79^{a}
相关系数 r		0.887		0.930		0.940		0.862	

注：同列数据后不同字母表示处理间差异达 $P < 0.05$ 显著水平。

叭口期到成熟期，夏玉米地上干物质量均呈现逐渐升高的变化趋势，而全氮含量则呈逐渐下降趋势。吐丝期到灌浆期是玉米吸收和积累营养的高峰期。从吐丝期开始，植株体内储藏性养分开始向玉米雌穗转移，降低了同化速率[29]，所以灌浆期后地上干物质量增长速度有所下降，不同施肥处理具有相似的变化趋势[30]。

在相同磷肥水平下，随着施氮量增加，地上干物质量均有显著增长（$P < 0.05$），Al Abbas 等的研究也证明了增施氮肥可显著增加地上干物质量[31]。在相同氮肥水平下，随着施磷量增加，地上干物质量也有所增长。高氮高磷耦合处理（P2N3、P2N4、P3N3、P3N4）地上干物质量均高于低氮低磷耦合处理（P0N0、P0N1、P1N0、P1N1）。如吐丝期高氮高磷耦合处理与低氮低磷耦合处理条件下，地上干物质量分别相差 6.88、5.35、6.43、5.80 t/hm^2，全氮质量分数差值分别为 0.83%、0.58%、0.77%、0.69%。

在各生育时期，地上干物质量与氮素含量有较高的相关系数，表明二者在氮磷耦合处理影响下，有相似的变化趋势，均随施肥量的增高而增加，且有显著的差异。

2.2　不同氮磷施肥水平下的夏玉米冠层光谱反射率

以 2013 年郑单 958 吐丝期夏玉米冠层光谱反射率为例，分析不同氮磷施肥水平下夏玉米冠层光谱反射率变化趋势，如图 1 所示。不同氮磷营养水平下，夏玉米冠层反射光谱在 350 ~ 2 350 nm 波段走势基本一致。在 350 ~ 680 nm 波段，光谱反射率较低；在 550 nm 左右为叶绿素强反射峰（绿峰），光谱反射率在 8% ~ 12%。在 680 nm 左右为吸收谷，是参与光合作用的叶绿素吸收红光的结果。在 680 ~ 750 nm 波段，光谱反射率直线上升，为绿色植物的特征光谱“红边”，红光波段叶绿素的强烈吸收与近红外波段光在叶片内部多次散射形成了该波段特征，此特征是描述作物健康状况的重要指标。在近红外波段（750 ~ 1 150 nm）有一稳定反射平台，冠层光谱反射率趋于稳定（36% ~ 42%）。在 1 150 ~ 2 350 nm光谱反射率逐渐下降，并且在 1 700 nm 和 2 200 nm左右有 2 个反射峰；在 1 400 nm 和 1 900 nm 左右为水分全吸收波段，由于受水汽影响较大，已剔除。

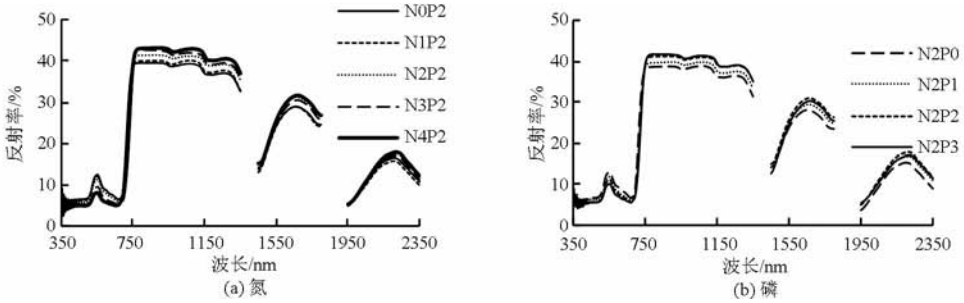

图 1　不同氮、磷施肥水平下夏玉米冠层光谱反射率变化曲线

Fig. 1　Change of canopy spectral reflectance of summer maize under different N, P application rates

不同氮、磷施肥水平下，夏玉米冠层反射光谱响应曲线变化趋势较为相似。在可见光波段（350 ~ 680 nm），光谱反射率随施氮量和施磷量增加而降低；在近红外波段（750 ~ 1 350 nm），光谱反射率随施氮量和施磷量增加而升高；在 1 350 nm 之后，光谱反射率与氮磷肥力梯度无明显响应规律。

2.3　冠层光谱反射率与地上干物质量及全氮含量的相关性

将 2011—2012 年独立光谱反射率实验数据及其地上干物质量进行相关分析（图 2），可知夏玉米冠层反射光谱与地上干物质量的相关性变化动态。从图 2 可看出，在 350 ~ 2 350 nm 光谱范围内，光谱反射率与地上干物质量和全氮含量相关性曲线走势相似，且相关系数均差异不大，进一步表明地上干物质量和氮素含量与光谱反射率的相关关系具有较高的相似性。

在 430 ~ 720 nm 波段，夏玉米冠层原始光谱反射率与地上干物质量具有较高的负相关性，形成一个比较稳定的平台，相关系数分别为 -0.593 ~ -0.687。在红边位置，所有的相关系数均有较明显的波动，且随着波长的增加，相关性由显著负相关逐

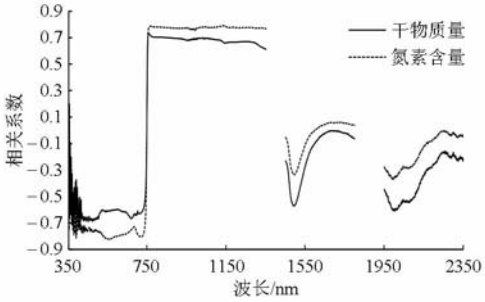

图 2　夏玉米地上干物质量与冠层原始光谱反射率的相关系数随波长的变化动态

Fig. 2　Correlation coefficient between original spectral reflectance and ADMA, N content of summer maize canopy at different growth stages of maize

渐转变为显著正相关。在 750 ~ 1 350 nm 波段,夏玉米冠层原始光谱反射率与地上干物质量的相关系数为 0.578 ~ 0.733。表 1 中所选植被指数的波段,均在 430 ~ 720 nm 和 750 ~ 1 350 nm 稳定相关系数波段平台内。

2.4 玉米地上干物质量光谱监测模型构建

选择 2011 年和 2013 年夏玉米地上干物质量与相对应的植被指数(n = 240,5 种氮肥梯度、4 种磷肥梯度、3 个重复及 2 年实验),基于不同生育时期建立监测模型(表 3)。本文选择线性函数、对数函数、二次函数、指数函数与 21 种植被指数变量拟合回归模型,并计算分析地上干物质量拟合模型的精度变化(决定系数 R^2 及 F 值)。基于同一个植被指数所建立的 4 种模型中,二次函数模型普遍具有较高的决定系数。线性、对数及指数拟合模型具有较为相近的决定系数和方程参数。

对于作物生理生态参数估算模型选择,不仅要求回归模型的决定系数和 F 值均要高,而且需要具有可重复性。从表 3 中,每个生育时期分别选取决定系数和 F 值较高的 3 个拟合模型进行精度检验分析(表 4)。在大喇叭口期,夏玉米地上干物质量的拟合模型决定系数均不高,可能是由于夏玉米叶面积指数小,土壤背景干扰较大。在吐丝期,回归模型决定系数和 F 值均有所提高,且地上干物质量与植被指数 PSSRc 和 MTCI 有较高的模型决定系数。在灌浆期,地上干物质量与植被指数 GNDVI 和 NDVI4 组建的模型具有较高的决定系数,因此选为较适模型以便进行进一步精度检验。在成熟期,地上干物质量与植被指数 DI 组建的模型有最高的决定系数和较高的 F 值。

表 3 夏玉米不同生育时期地上干物质量与植被指数回归模型参数

Tab.3 Parameters of regression models between ADMA and vegetation index of summer maize at different growth stages

植被指数	回归模型	大喇叭口期		吐丝期		灌浆期		成熟期	
		R^2	F	R^2	F	R^2	F	R^2	F
GI	线性	0.098	0.655	0.041	0.254	0.244	1.932	0.281	2.350
	对数	0.099	0.658	0.037	0.229	0.251	2.011	0.278	2.312
	二次	0.099	0.276	0.143	0.419	0.270	0.924	0.318	1.164
	指数	0.110	0.738	0.041	0.254	0.222	1.714	0.297	2.535
PSSRa	线性	0.688	13.234	0.453	4.965	0.323	2.861	0.491	5.799
	对数	0.697	13.795	0.551	7.377	0.366	3.459	0.502	6.056
	二次	0.734	6.892	0.716	17.179	0.424	1.843	0.541	2.942
	指数	0.666	11.955	0.461	5.141	0.345	3.158	0.477	5.469
PSSRb	线性	0.548	7.285	0.536	6.942	0.434	4.608	0.768	19.850
	对数	0.611	9.433	0.640	10.682	0.500	5.997	0.777	20.906
	二次	0.849	26.292	0.840	28.879	0.583	3.501	0.784	9.089
	指数	0.545	7.180	0.544	7.172	0.453	4.974	0.759	18.888
PSSRc	线性	0.616	9.628	0.449	4.890	0.345	3.164	0.532	6.809
	对数	0.642	10.761	0.557	7.546	0.390	3.842	0.544	7.169
	二次	0.749	7.452	0.857	35.487	0.439	1.954	0.582	3.477
	指数	0.601	9.055	0.457	5.056	0.369	3.506	0.505	6.125
SRPI	线性	0.192	1.427	0.001	0.007	0.004	0.024	0.114	0.771
	对数	0.186	1.375	0.002	0.010	0.003	0.021	0.114	0.772
	二次	0.315	1.152	0.554	3.104	0.181	0.554	0.114	0.321
	指数	0.194	1.440	0.003	0.016	0.002	0.015	0.091	0.603
DI	线性	0.675	12.446	0.666	11.957	0.755	18.469	0.884	45.590
	对数	0.707	14.466	0.699	13.921	0.771	20.163	0.891	49.008
	二次	0.766	71.332	0.806	10.354	0.797	9.829	0.897	26.184
	指数	0.673	12.359	0.684	12.982	0.772	20.290	0.887	47.284
DVI	线性	0.791	22.669	0.617	9.653	0.514	6.345	0.840	31.549
	对数	0.800	24.072	0.645	10.908	0.529	6.736	0.844	32.501
	二次	0.802	20.788	0.811	10.732	0.585	3.525	0.858	15.145
	指数	0.857	37.169	0.634	10.405	0.536	6.927	0.840	31.532
DD	线性	0.805	24.808	0.767	19.709	0.704	14.250	0.726	15.881
	对数	0.811	25.676	0.725	15.800	0.624	9.950	0.748	17.798
	二次	0.815	11.006	0.767	8.213	0.708	6.049	0.761	7.962
	指数	0.814	26.270	0.792	22.856	0.714	15.008	0.750	18.015

续表 3

植被指数	回归模型	大喇叭口期		吐丝期		灌浆期		成熟期	
		R^2	F	R^2	F	R^2	F	R^2	F
MTCI	线性	0.721	15.498	0.802	24.316	0.657	11.493	0.663	11.798
	对数	0.769	19.935	0.781	21.441	0.652	11.253	0.717	15.202
	二次	0.804	10.271	0.802	10.137	0.663	4.927	0.797	9.793
	指数	0.724	15.757	0.863	27.840	0.660	11.649	0.683	12.955
GNDVI	线性	0.589	8.591	0.710	14.668	0.791	22.726	0.861	37.211
	对数	0.626	10.060	0.740	17.052	0.799	23.810	0.871	40.531
	二次	0.851	38.799	0.840	13.144	0.806	10.404	0.878	27.135
	指数	0.591	8.659	0.725	15.833	0.809	25.488	0.861	37.125
NPCI	线性	0.187	1.378	0.002	0.010	0.003	0.021	0.114	0.772
	对数	0.242	1.920	0.020	0.123	0.015	0.090	0.134	0.929
	二次	0.315	1.149	0.557	3.137	0.178	0.541	0.114	0.323
	指数	0.189	1.395	0.003	0.021	0.002	0.012	0.091	0.603
NPQI	线性	0.100	0.670	0.012	0.071	0.311	2.702	0.025	0.156
	对数	—	—	—	—	—	—	—	—
	二次	0.477	2.278	0.222	0.713	0.436	1.929	0.027	0.070
	指数	0.088	0.578	0.013	0.076	0.302	2.600	0.031	0.191
PRI	线性	0.337	3.046	0.700	13.999	0.219	1.682	0.031	0.190
	对数	0.384	3.733	0.714	14.968	0.259	2.092	0.020	0.121
	二次	0.430	1.885	0.723	6.529	0.258	0.868	0.236	0.773
	指数	0.377	3.626	0.672	12.310	0.239	1.889	0.025	0.151
SIPI	线性	0.013	0.081	0.185	1.363	0.006	0.034	0.094	0.625
	对数	0.014	0.082	0.184	1.357	0.006	0.033	0.094	0.621
	二次	0.013	0.081	0.186	1.368	0.006	0.035	0.095	0.628
	指数	0.018	0.109	0.205	1.546	0.007	0.043	0.075	0.490
MSR705	线性	0.760	19.001	0.794	23.154	0.769	19.963	0.528	6.703
	对数	0.761	19.076	0.765	19.577	0.753	18.299	0.576	8.145
	二次	0.762	7.992	0.804	10.266	0.770	8.391	0.676	5.217
	指数	0.762	19.261	0.817	26.798	0.762	19.160	0.556	7.499
PSRI	线性	0.192	1.426	0.780	21.283	0.381	3.694	0.485	5.649
	对数	—	—	—	—	—	—	—	—
	二次	0.237	0.777	0.784	9.075	0.405	1.705	0.848	13.936
	指数	0.198	1.481	0.804	24.580	0.386	3.771	0.478	5.492
RGR	线性	0.040	0.247	0.301	2.587	0.042	0.261	0.111	0.746
	对数	0.039	0.241	0.301	2.586	0.040	0.251	0.111	0.752
	二次	0.064	0.172	0.301	1.078	0.069	0.185	0.123	0.350
	指数	0.046	0.287	0.298	2.553	0.033	0.202	0.118	0.802
NDVI1	线性	0.824	28.164	0.766	19.660	0.627	10.086	0.779	21.134
	对数	0.837	30.921	0.769	19.934	0.617	9.658	0.790	22.522
	二次	0.853	14.454	0.773	8.491	0.627	4.203	0.805	10.321
	指数	0.830	29.197	0.790	22.535	0.643	10.803	0.796	23.456
NDVI2	线性	0.621	9.830	0.720	15.458	0.622	9.882	0.839	31.335
	对数	0.644	10.849	0.743	17.379	0.626	10.028	0.842	32.016
	二次	0.805	13.935	0.835	12.671	0.629	4.241	0.848	13.898
	指数	0.619	9.764	0.735	16.642	0.645	10.899	0.839	31.270
NDVI3	线性	0.699	13.903	0.618	9.703	0.378	3.652	0.526	6.648
	对数	0.701	14.060	0.640	10.662	0.385	3.757	0.529	6.749
	二次	0.699	13.903	0.843	13.395	0.400	1.664	0.574	3.363
	指数	0.677	12.564	0.630	10.218	0.405	4.086	0.514	6.347
NDVI4	线性	0.590	8.619	0.711	14.753	0.796	23.369	0.856	35.791
	对数	0.627	10.079	0.741	17.126	0.802	24.379	0.867	39.026
	二次	0.850	47.507	0.839	13.003	0.809	10.599	0.870	27.117
	指数	0.591	8.677	0.726	15.929	0.814	26.237	0.856	35.691

注：“—”表示自变量包含非正数值，无法计算对数函数模型。

表 4 夏玉米不同生育时期地上干物质量与植被指数回归模型验证

Tab. 4 Verification of regression models between ADMA and vegetation index of summer maize at different growth stages

生育时期	植被指数	拟合模型	均方根差/(t·hm^{-2})	相对误差/%
大喇叭口期	DVI	$y=1.164e^{0.336x}$	2.096	10.85
	GNDVI	$y=-190.298+659x-520.752x^2$	0.945	5.53
	NDVI1	$y=-29.000+149.782x-116.928x^2$	1.644	9.23
吐丝期	PSSRc	$y=-20.977+9.796x-0.501x^2$	1.044	3.93
	MTCI	$y=14.834e^{0.007x}$	2.246	7.54
	NDVI3	$y=-367.796+976.526x-605.895x^2$	1.994	7.52
灌浆期	GNDVI	$y=16.183e^{0.081x}$	5.473	10.57
	NDVI4	$y=-41.278+238.043x-148.690x^2$	5.013	11.05
	NDVI4	$y=16.104e^{0.082x}$	5.408	10.47
成熟期	DI	$y=130.535+68.978\ln x$	2.175	4.932
	DI	$y=-276.451+1\,979.524x-2\,982.515x^2$	2.234	5.516
	DI	$y=11.254e^{5.312x}$	1.761	4.578

2.5 夏玉米地上干物质量光谱监测模型精度检验

为了检验监测模型的稳定性及可靠性,利用 2012 年和 2014 年夏玉米各生育时期实验独立数据($n=240$)进行均方根差(RMSE)和相对误差(RE)的测试。从每个生育时期分别选择 3 个决定系数和 F 值较高的模型进行地上干物质量模型精度检验,并选择均方根差和相对误差均较低的模型为最适模型,此模型具有较好的稳定性和可重复性。结果表明,地上干物质量与植被指数 GNDVI、PSSRc、NDVI4 和 DI 建立的模型为最适模型。

3 讨论

研究作物地上干物质量状况,传统方法多采用实地测量作物叶片及鲜干物质量,不仅费时费力,而且对作物有破坏性。遥感技术可以对作物冠层快速有效、非破坏性地进行田间信息采集与处理,实现作物大面积快速、准确检测。

已有的研究多偏重于成熟期的地上干物质量模型拟合[32-33],较少对作物生育前中期进行相应的研究。本实验通过对夏玉米不同生育时期及多种波段构建的植被指数与地上干物质量建立了拟合模型,并进行了相应的精度检验,从统计学角度分析了地上干物质量与冠层反射光谱的关系,并建立了与之相对应的监测模型,为大田玉米生长监测与实时诊断提供了量化指标。

相比宽波段植被指数,窄波段植被指数更容易受仪器、环境噪声和背景等的影响,这可能是造成研究结果差异的重要原因。实验结果表明,波段组合的植被指数可有效降低上述误差,提高模型的精准度[34-36]。

在不同生育时期选择的 12 个模型中(表 4),含有 800 nm 和 550 nm 参量的模型分别有 7 个。在已有的众多研究论述中,800 nm 和 550 nm 波段参量被用于众多植被指数的频率较高,且已应用于多种植物的长势监测,但对夏玉米不同生育时期长势监测的研究相对较少。本文对不同生育时期夏玉米地上生物量与多种光谱植被指数进行了相关性分析,并进行了相关的模型验证。结果表明,在夏玉米不同的生育时期,光谱敏感波段有一定的差异,植被指数的选择也因此而不同;在生物量较高的生育后期,DI 有较高的决定系数和 F 值,且具有较小的均方根差和相对误差。

在生育前中期(大喇叭口期、吐丝期和灌浆期)选择的 9 个模型中,植被指数为 NDVI 和 GNDVI 参量的模型分别有 4 个和 2 个,这 2 种模型已广泛应用于氮素、LAI 和生物量等的模型构建中。但在生育后期(成熟期),DI 植被指数较好地解决了 NDVI 算式本身存在的容易饱和的缺陷[28,37]。

本研究中,在成熟期所建立的最适模型地上干物质量均为基于植被指数 DI 的指数函数模型,这与前人的研究结论相似[38-39],且此生育时期的其他 DI 验证模型也均具有较低均方根差和相对误差,基于植被指数 DI 建立的模型均具有较好的稳定性和较高精度。由于已有的关于地上干物质量研究多偏重于成熟期,且成熟期的地上干物质量研究具有重要的应用价值,所以关于成熟期的相关模型建立也显得尤为重要,且具有较高的实用意义。

本实验基于不同的生育时期对夏玉米地上干物质量进行了光谱植被指数拟合分析,不同生育时期的最佳植被指数具有较大差异,尚未发现可应用于监测所有生育时期的植被指数,对于普适于所有生育时期的光谱监测干物质量的模型还有待于进一步研究。

4　结论

(1)在不同施肥量条件下,夏玉米冠层地上干物质量和全氮含量均有明显差异,各生育时期全氮含量逐渐下降,地上干物质量逐渐上升。冠层光谱反射率与全氮含量和地上干物质量均具有较强的相关性。

(2)在大喇叭口期、吐丝期、灌浆期和成熟期,夏玉米地上干物质量的最优预测模型分别为:$y = -190.298 + 659x - 520.752x^2$(GNDVI)、$y = -20.977 + 9.796x - 0.501x^2$(PSSRc)、$y = 16.104e^{0.082x}$(NDVI4)和 $y = 11.254e^{5.312x}$(DI)。

参　考　文　献

1　赵英时. 遥感应用分析原理与方法[M]. 北京:科学出版社,2003.

2　张良培,郑兰芬,童庆禧. 利用高光谱数据对生物变量进行估计[J]. 遥感学报,1997,1(2):111 - 114.
ZHANG Liangpei, ZHENG Lanfen, TONG Qingxi. The estimation of vegetation variables based on high resolution spectra[J]. Journal of Remote Sensing, 1997,1(2):110 - 114. (in Chinese)

3　王渊,王福民,黄敬峰. 油菜不同组分生物量光谱遥感估测模型[J]. 浙江农业学报,2004,16(2):79 - 83.
WANG Yuan, WANG Fumin, HUANG Jingfeng. The models for estimation of dry biomass from different components of rapeseed using canopy spectral data[J]. Acta Agriculturae Zhejiangensis, 2004,16(2):79 - 83. (in Chinese)

4　SHIBAYAMA M, AKIYAMA T. Seasonal visible nearinfrared and midinfrared spectra of rice canopies in relation to LAI and aboveground dry biomass[J]. Remote Sensing of Environment,1989,27(2):119 - 197.

5　宋开山,张柏,李方,等. 高光谱反射率与大豆叶面积及地上鲜物质积累量的相关分析[J]. 农业工程学报,2005,21(1):36 - 40.
SONG Kaishan, ZHANG Bai, LI Fang, et al. Correlative analyses of hyperspectral reflectance, soybean LAI and aboveground biomass[J]. Transactions of the CSAE, 2005,21(1):36 - 40. (in Chinese)

6　庄东英,李卫国,武立权. 冬小麦生物量卫星遥感估测研究[J]. 干旱区资源与环境,2013,27(10): 158 - 162.
ZHUANG Dongying, LI Weiguo, WU Liquan. Estimating winter wheat biomass based on satellite remote sensing[J]. Journal of Arid Land Resources and Environment, 2013,27(10): 158 - 162. (in Chinese)

7　除多,德吉央宗,普布次仁,等. 藏北草地地上生物量及遥感监测模型研究[J]. 自然资源学报,2013,28(11):2000 - 2011.
CHU Duo, DEJI Yangzong, PUBU Ciren, et al. Aboveground biomass in the north Tibet and estimate model using remote sensing data[J]. Journal of Natural Resource, 2013,28(11): 2000 - 2011. (in Chinese)

8　付元元,王纪华,杨贵军,等. 应用波段深度分析和偏最小二乘回归的冬小麦生物量高光谱估算[J]. 光谱学与光谱分析,2013,33(5): 1315 - 1319.
FU Yuanyuan, WANG Jihua, YANG Guijun, et al. Band depth analysis and partial least square regression based winter wheat biomass estimation using hyperspectral measurements[J]. Spectroscopy and Spectral Analysis, 2013,33(5):1315 - 1319. (in Chinese)

9　TOMPPO E, NILSSON M, ROSENGREN M. Simultaneous use of landsat-TM and IRS - 1C WiFS data in estimating large area tree stem volume and aboveground biomass[J]. Remote Sensing of Environment,2002,82(1):156 - 171.

10　SPANNER M, JOHNSON L, MILLER J, et al. Remote sensing of seasonal leaf-area index across the oregon transect [J]. Ecological Applications,1994,4(2):258 - 271.

11　YANG Y H,FANG J Y,PAN Y D,et al. Aboveground biomass in Tibetan grasslands[J]. Journal of Arid Environments,2009, 73(1): 91 - 95.

12　CHOUDHURY B J. Relationships between vegetation indices, radiation absorption and net photosynthesis evaluated by a sensitivity analysis[J]. Remoting Sensing Environment, 1987, 22(2): 209 - 233.

13　SMITH R C G, ADAMS J, STEPHENS D J, et al. Forecasting wheat yield in a mediterranean-type environment from the NOAA satellite[J]. Australian Journal of Agricultural Research,1995, 46(1):113 - 125.

14　BLACKBURN G A. Quantifying chlorophylls and carotenoids at leaf and canopy scales: an evaluationof some hyperspectral approaches[J]. Remote Sensing of Environment, 1998,66(3):273 - 285.

15　PENUELAS J, GAMON J A, FREDEEN A L, et al. Reflectance indices associated with physiological changes in nitrogen-limited and water-limited sunflower leaves[J]. Remote Sensing of Environment, 1994,48(2):135 - 146.

16　BUSCHMAN C, NAGEL E. In vivo spectroscopy and internal optics of leaves as a basis for remote sensing of vegetation[J]. International Journal of Remote Sensing, 1993,14(4):711 - 722.

17　JORDAN C F. Derivation of leaf area index from quality of light on the forest floor[J]. Ecology, 1969,50(4):663 - 666.

18　LE MAIRE G, FRANçOIS C, DUFRENE E. Towards universal broad leaf chlorophyll indices using PROSPECT simulated database and hyperspectral reflectance measurements[J]. Remote Sensing of Environment, 2004,89(1):1 - 28.

19　DASH J, CURRAN P J. The MERIS terrestrial chlorophyll index[J]. International Journal of Remote Sensing, 2004,25(23):5403 - 5413.

20　DAUGHTRY C S T, WALTHALL C L, KIM M S, et al. Estimating corn leaf chlorophyll concentration from leaf and canopy reflectance[J]. Remote Sensing of Environment, 2000,74(2):229 - 239.

21 PENUELAS J, BARET F, FILELLA I. Semi-empirical indices to assess carotenoids/chlorophyll a ratio from leaf spectral reflectance[J]. Photosynthetica, 1995,31:221 - 230.

22 BARNES J D, BALAGUER L, MANRIQUE E, et al. A reappraisal of the use of DMSO for the extraction and determination of chlorophylls-a and chlorophylls-b in lichens and higher plants[J]. Environmental and Experimental Botany, 1992,32(2):85 - 100.

23 GAMON J A, PENUELAS J, FIELD C B. A narrow-waveband spectral index that tracks diurnal changes in photosynthetic efficiency[J]. Remote Sensing of Environment, 1992, 41(1):35 - 44.

24 SIMS D A, GAMON J A. Relationships between leaf pigment content and spectral reflectance across a wide range of species, leaf structures and developmental stages[J]. Remote Sensing of Environment, 2002,81(2 - 3): 337 - 354.

25 STEDDOM K, HEIDEL G, JONES D, et al. Remote detection of rhizomania in sugar beets[J]. Phytopathology, 2003,93(6): 720 - 726.

26 MA B L, MORRISON M J, DWYER L M. Canopy light reflectance and field greenness to assess nitrogen fertilization and yield of maize[J]. Agronomy Journal, 1996,88(6):915 - 920.

27 SERRANO L, FILELLA I, PENUELAS J. Remote sensing of biomass and yield of winter wheat under different nitrogen supplies [J]. Crop Science, 2000,40(3):723 - 731.

28 GITELSON A A, KAUFMAN Y J, MERZLYAK M N. Use of a green channel in remote sensing of global vegetation from EOS - MODIS[J]. Remote Sensing of Environment, 1996,58(3):289 - 298.

29 申丽霞,王璞,张软斌. 施氮对不同种植密度下夏玉米产量及子粒灌浆的影响[J]. 植物营养与肥料学报,2005,11(3): 314 - 319.
SHEN Lixia, WANG Pu, ZHANG Ruanbin. Effect of nitrogen supply on yield and grain filling in summer maize with different crop density[J]. Plant Nutrition and Fetilizer Science, 2005,11(3):314 - 319. (in Chinese)

30 党红凯,李伟,曹彩云,等. 乳熟后灌溉对夏玉米水分利用效率及干物质转运的影响[J]. 农业机械学报, 2014,45(5): 131 - 138.
DANG Hongkai, LI Wei, CAO Caiyun, et al. Effect of late milk irrigation on water use efficiency and dry matter distribution of maize[J]. Transactions of the Chinese Society for Agricultural Machinery, 2014,45(5): 131 - 138. (in Chinese)

31 AL ABBAS A H, BARR R, HALL J D. Spectra of normal and nutrient-deficient maize leaves[J]. Agronomy Journal, 1974,66 (1): 16 - 20.

32 QI J, CABOT F, MORAN M S, et al. Biophysical parameter estimations using multidirectional spectral measurements[J]. Remote Sensing of Environment, 1995,54(1):71 - 83.

33 JACQUEMOUD S, BACOUR C, POILVE H, et al. Comparison of four radiative transfer models to simulate plant canopies reflectance: direct and inverse mode[J]. Remote Sensing of Environment, 2000,74(3):471 - 481.

34 DENTE L, SATALINO G, MATTIA F, et al. Assimilation of leaf area index derived from ASAR and MERIS data into CERES - Wheat model to map wheat yield[J]. Remote Sensing of Environment, 2008, 112(4): 1395 - 1407.

35 WIT A D, DUVEILLER G, DEFOURNY P. Estimating regional winter wheat yield with WOFOST through the assimilation of green area index retrieved from MODIS observations[J]. Agricultural and Forest Meteorology, 2012, 164(6): 39 - 52.

36 MANGIAROTTI S, MAZZEGA P, JARLAN L, et al. Evolutionary bi-objective optimization of a semi-arid vegetation dynamics model with NDVI and σ_0 satellite data[J]. Remote Sensing of Environment, 2008, 112(4): 1365 - 1380.

37 TANG Y L, WANG R C, HUANG J F. Relations between red edge characteristics and agronomic parameters of crops[J]. Pedosphere, 2004,14(4):467 - 474.

38 RAUSTE Y. Multi-temporal JERS SAR data in boreal forest biomass mapping[J]. Remote Sensing of Environment, 2005,97(2): 263 - 275.

39 LUCAS R M, CRONIN N, LEE A, et al. Empirical relationships between AIRSAR backscatter and LiDAR-derived forest biomass, Queensland, Australia[J]. Remote Sensing of Environment, 2006,100(3):407 - 425.